Two-dimensional non-Hermitian topological phases induced by asymmetric hopping in a one-dimensional superlattice

Junpeng Hou,[1] Ya-Jie Wu,[1,2] and Chuanwei Zhang[1,*]
[1]*Department of Physics, The University of Texas at Dallas, Richardson, Texas 75080-3021, USA*
[2]*School of Science, Xi'an Technological University, Xi'an 710032, China*

(Received 14 May 2020; revised 7 January 2021; accepted 28 January 2021; published 5 March 2021)

Non-Hermitian systems can host topological states with unusual topological invariants and bulk-edge correspondences that are distinct from conventional Hermitian systems. Here we show that two unique classes of non-Hermitian two-dimensional topological phases, a $2\mathbb{Z}$ non-Hermitian Chern insulator and a $\mathbb{Z}_2$ topological semimetal, can be realized by solely tuning staggered non-Hermitian or asymmetric hopping strengths in a one-dimensional (1D) superlattice. These non-Hermitian topological phases support real edge modes due to robust $\mathcal{PT}$-symmetric-like spectra and can coexist in a certain parameter regime. The proposed phases can be experimentally realized in photonic or atomic systems and may open an avenue for exploring unique classes of non-Hermitian topological phases with 1D superlattices.

DOI: 10.1103/PhysRevA.103.033305

I. INTRODUCTION

In the past few decades, topological states of matter have been extensively studied in various physical systems because of their unusual properties and significant applications in quantum devices and information processing [1,2]. While the study has mainly focused on solid-state materials [3], ultracold atomic gases provide another platform for realizing topological states with high tunability and controllability [4–11] . Furthermore, the concept of topology has been extended to classical systems govern by wave equations such as photonics [12–18], acoustics [19,20], and electric circuits [21], yielding many interesting topological states.

One significant feature of ultracold atomic gases and these classical systems comparing to quantum materials is their capability of controllably inducing non-Hermiticity (e.g., gain and loss), which makes them excellent platforms for exploring distinct non-Hermitian physics, such as unidirectional transportation [22], spontaneous $\mathcal{PT}$-symmetry breaking with exceptional points [23,24], fast eigenstate transition [25], and exotic superfluidity [26,27], etc. In particular, significant effects and applications have been proposed or demonstrated in non-Hermitian photonics [28–33].

The combination of topology and non-Hermiticity leads to the emergence of unusual topological effects, such as anomalous edge states, non-Bloch waves, non-Hermitian skin effects, etc. [34–42]. In experiments, photonic [43–51] and atomic [52,53] systems are leading platforms for realizing non-Hermitian topological states. Although in most work the non-trivial topology is attributed to the Hermitian part of the Hamiltonian, it has been recently proposed that topological states may be solely induced by non-Hermiticity [47] with a focus on higher-order topological insulators [51,53,54]. The classification of non-Hermitian topological phases has been proposed through a reduction from AZ classes [55], which remains incomplete because a random non-Hermitian matrix belongs to a broader BL class [56]. More recently, a comprehensive classification of non-Hermitian systems has been achieved through introducing the complex AZ† class [57].

In Hermitian systems, it is known that two-dimensional (2D) topological phases, such as a Chern insulator, can be simulated using a one-dimensional (1D) lattice with staggered hopping or onsite potential [58] characterized by an additional periodic parameter. The experimental realization of such 2D topological phases in momentum-parameter space could be significantly simpler, comparing to their 2D lattice counterparts. In this context, two natural questions arise for non-Hermitian systems: (i) Can 2D non-Hermitian topological phases be realized using 1D lattices with solely non-Hermitian effects? (2) If so, is there any unique class of non-Hermitian topological phases that are difficult to realize in Hermitian systems?

In this work, we address these two important questions by showing that two unique symmetry-protected non-Hermitian topological phases can be realized in a 1D superlattice with staggered asymmetric hopping. Our main results are as follows:

(i) The 1D superlattice hosts a 2D topological insulator phase characterized by a $2\mathbb{Z}$ Chern number, which is protected by certain symmetry that is unique to non-Hermitian systems [56]. Such a phase is difficult to access in Hermitian systems because it is absent in the AZ classification and requires a crystalline symmetry as well as a global $\mathbb{Z}_2$ symmetry [59].

(ii) A topological semimetal phase hosting complex Dirac points and zero-energy modes is found to be associated with a $\mathbb{Z}_2$ invariant, which is extracted from the normalized Berry phase for non-Hermitian systems.

(iii) The system may support edge states with real energy due to a robust $\mathcal{PT}$-symmetric-like phase. In most

*chuanwei.zhang@utdallas.edu

non-Hermitian systems with onsite gain and loss, the $\mathcal{PT}$-symmetric phase becomes fragile with increasing system size. In contrast, the $\mathcal{PT}$-symmetric-like phase here is robust to varying chain length. Furthermore, these two topological phases can coexist in proper parameter spaces.

(iv) Our model is topologically trivial when there are only Hermitian terms. The topological phases here are induced by only non-Hermitian asymmetric hopping. This feature distinguishes our work from previous work studying a non-Hermitian Aubry-André-Harper model [60], where the model is topological when the non-Hermitian effects vanish. Our work reveals that even pure non-Hermiticity in 1D could generate nontrivial topological phases in 2D.

II. 2D NON-HERMITIAN TOPOLOGICAL PHASES IN 1D SUPERLATTICE WITH ASYMMETRIC HOPPING

A. Model Hamiltonian

We consider a lattice model with nearest-neighbor hopping, which can be described by a tight-binding Hamiltonian

$$H_r = \sum_j (t_{j,j+1}\hat{c}_j^\dagger \hat{c}_{j+1} + t_{j+1,j}\hat{c}_{j+1}^\dagger \hat{c}_j) + V_j \hat{c}_j^\dagger \hat{c}_j. \quad (1)$$

Here, $\hat{c}_j^\dagger$ ($\hat{c}_j$) is the creation (annihilation) operator of local modes at site j, and the hopping term is asymmetric $t_{j,j+1} \neq t_{j+1,j}^*$. For simplicity of the presentation, we assume uniform onsite potential and staggered hopping terms

$$t_{j,j+1} = t_0 + \lambda \cos(2\pi\alpha j + \phi_L), \quad (2)$$

$$t_{j+1,j} = t_0 - \lambda \cos(2\pi\alpha j + \phi_L), \quad (3)$$

where $\lambda, \alpha \in \mathbb{R}$ and we choose $t_0 = 1$ as the energy unit. If we consider only two nearest-neighbor sites j and $j+1$ in the chain, the Hamiltonian for the subsystem is $\sigma_x + i\sigma_y \cos(2\pi\alpha j + \phi_L)$, where the imaginary unit appears and σ_j are Pauli matrices.

We consider rational α that can be written as the quotient of two relatively prime integers $\alpha = p/q$, $p, q \in \mathbb{Z}$. Without loss of generality, p, q are assumed to be positive and $p < \lceil q/2 \rceil$. The corresponding Bloch Hamiltonian $H(k, \phi_L)$ for the superlattice is a $q \times q$ matrix in the Brillouin zone $|k| \leqslant \pi/q$ with nonzero entries $H_{j,j} = V_j$, $H_{j,j+1} = t_{j,j+1}$, $H_{j+1,j} = t_{j+1,j}$ for $j+1 < q$, $H_{1,q} = t_{1,q}e^{-iqk}$, and $H_{q,1} = t_{q,1}e^{iqk}$.

The resulting Bloch Hamiltonian $H(k, \phi_L)$ preserves time-reversal symmetry $\mathcal{T}_k H(k, \phi_L)\mathcal{T}_k^{-1} = H^*(k, \phi_L) = H(-k, \phi_L)$ with $\mathcal{T}_k = K$ and K the complex conjugate, therefore, the real (complex) part of the band is symmetric (antisymmetric) about $k = 0$. Another symmetry reads as $\mathcal{P}_{\phi_L} H(k, \phi_L)\mathcal{P}_{\phi_L}^{-1} = H^T(k, -\phi_L)$, where $\mathcal{P}_{\phi_L}$ has a permutation representation $(q, 1)(q-1, 2)(q-2, 3)\ldots$ in 2-cycle forms.

B. 2$\mathbb{Z}$ Chern insulator

We start with the simplest case $\alpha = \frac{1}{3}$, which represents a Chern insulator, as shown in Fig. 1(a). The Bloch band is gapped by its real part in the entire momentum space for any ϕ_L and exhibits the symmetry $\omega(k) = \omega^*(-k)$. We also plot the open-boundary spectrum with varying ϕ_L in

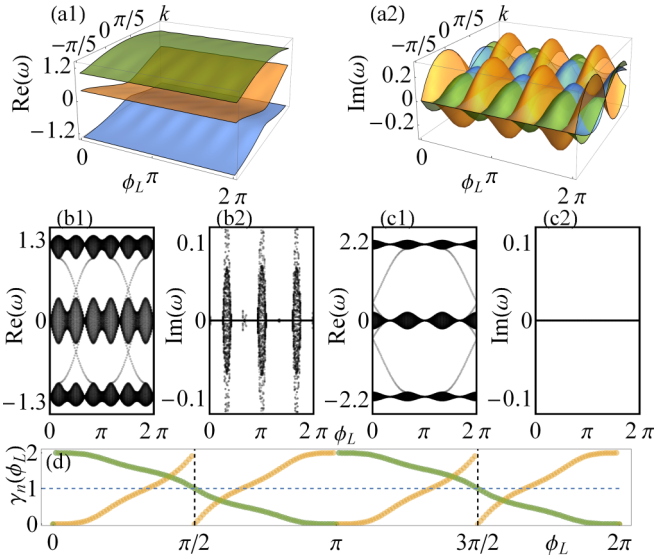

FIG. 1. 2$\mathbb{Z}$ Chern insulator phase when $\alpha = \frac{1}{3}$. (a) 2D band structure in momentum-parameter space when $\lambda = 1$. The Chern numbers for each band are -2, 4, and -2 (from bottom to top). (b) Open-boundary spectra with respect to ϕ_L for $\lambda = 1$ and $N_L = 120$. (c) Similar to (b) but plotted with $\delta\phi_L = \pi$, which leads to a $\mathbb{Z}$ Chern insulator with odd Chern number. (d) Normalized Berry phase $\gamma_n(\phi_L)$ for bulk bands in (b). The dashed vertical lines indicate inversion-symmetric points.

Fig. 1(b). Since the open-boundary Hamiltonian $H_O(\phi_L) = H_O^T(\phi_L + \pi)$, the spectrum is symmetric about $\phi_L = \pi$. When the lattice size satisfies $N_L/q \in \mathbb{Z}$, the Hamiltonian on a cylindrical geometry enjoys a sublattice symmetry $\mathcal{C}_O H_O(\phi_L)\mathcal{C}_O^{-1} = -H_O(\phi_L)$ with $\mathcal{C}_O = I_{N_L/q} \otimes \sigma_z$, where I_n is a $n \times n$ identity matrix. Thus, the open-boundary spectrum is symmetric about $\omega = 0$, as shown in Figs. 1(b) and 1(c). However, the spectra shown in Figs. 1(b) and 1(c) may not obey these symmetries exactly due to numeric errors, which are significantly enhanced when diagonalizing a non-Hermitian matrix.

Two pairs of "chiral" surface waves emerge in each gap [Fig. 1(b)] for varying ϕ_L. When $\alpha = \frac{1}{5}$, similar results with two or four pairs of edge modes in any of the four gaps are observed. In general, the number of the pair of edge states is always even, as expected for a 2$\mathbb{Z}$ Chern insulator phase. The Hamiltonian satisfies $H(k, \phi_L) = H^T(-k, \phi_L + \pi)$, which leads to $H(k, \phi_L) = H^\dagger(k, \phi_L + \pi)$ when combined with time-reversal symmetry, yielding the 2$\mathbb{Z}$ Chern insulator phase. When an extra term $\delta\phi_L \in \mathbb{R}$ is added in the asymmetric hopping $t_{i+1,i} = 1 - \lambda \cos(2\pi\alpha i + \phi_L + \delta\phi_L)$ that breaks this symmetry, only one pair of surface waves are observed in each gap, as shown in Fig. 1(c). We remark that the 2$\mathbb{Z}$ and the $\mathbb{Z}$ Chern insulator phases are distinct. The corresponding topological phase transition is demonstrated in Appendix A.

The above 1D physics mimics the 2D integer quantum Hall effect in the (k, ϕ_L) momentum-parameter space. The band topology can be characterized by the Chern number

$$C^{ab} = \frac{1}{2\pi} \int dk\, d\phi_L \left(\partial_k \mathcal{A}_{\phi_L}^{ab} - \partial_{\phi_L} \mathcal{A}_k^{ab}\right), \quad (4)$$

where $a, b = L, R$, the Berry connections are defined as $\mathcal{A}_k^{ab} = -i_a\langle\psi(k,\phi_L)|\partial_k\psi(k,\phi_L)\rangle_b$ and $\mathcal{A}_{\phi_L}^{ab} = -i_a\langle\psi(k,\phi_L)|\partial_{\phi_L}\psi(k,\phi_L)\rangle_b$, and the right and left eigenstates are defined as $H(k,\phi_L)|\psi(k,\phi_L)\rangle_R = \omega(k,\phi_L)|\psi(k,\phi_L)\rangle_R$ and $H^\dagger(k,\phi_L)|\psi(k,\phi_L)\rangle_L = \omega^*(k,\phi_L)|\psi(k,\phi_L)\rangle_L$. The four Chern numbers C^{ab} are equivalent [39] and C^{RL} is numerically found to be -2, 4, and -2 from bottom to top bands in Fig. 1(a). Thus, the bulk topological invariant agrees well with the edge states through usual bulk-edge correspondence. The Chern numbers are also consistent with the $2\mathbb{Z}$ Chern insulator and a mathematical proof of exact $2\mathbb{Z}$ quantization of Chern number can be found in Appendix B.

The edge states are also closely related to the 1D topology. When combining the $\mathcal{P}_{\phi_L}$ symmetry with $H(k,\phi_L) = H^T(-k,\phi_L+\pi)$, we obtain an inversion (glide) symmetry along k (ϕ_L), $\mathcal{I}_k H(k,\phi_L)\mathcal{I}_k^{-1} = H(-k,-\phi_L+\pi)$. Such a symmetry leads to high-symmetry points $\phi_L = \frac{\pi}{2}$ and $\frac{3}{2}\pi$, at which the edge states are degenerate and the corresponding 1D normalized Berry phase

$$\gamma_n(\phi_L) = \frac{1}{\pi}\oint dk\,\mathcal{A}_k^n \tag{5}$$

is quantized. Here, $\mathcal{A}_k^n = \frac{1}{2}(\mathcal{A}_k^{RL} + \mathcal{A}_k^{LR})$ and n represents band index (see Appendix B for details). We plot the Berry phase at different ϕ_L in Fig. 1(d) and the color for each band is the same as in Fig. 1(a). The top (green) and bottom (blue) bands have the same normalized Berry phases, so only the green one is visible.

We note that the normalized Berry phase is also quantized at $\phi_L = 0$ and π, which is not a coincidence, but a result of a symmetry $\mathcal{Q}H(k,\phi_L)\mathcal{Q}^{-1} = H^\dagger(-k,-\phi_L)$ with $\mathcal{Q} = \mathcal{P}_{\phi_L}\mathcal{T}_k$ (see Appendix B for details). A close observation reveals that $\gamma_n(\phi_L)$ shows a period π and is antisymmetric to $\phi_L = \pi$. Note that Fig. 1(d) also demonstrates a charge pumping process with respect to ϕ_L, where the accumulation of Berry phases from $\phi_L = 0$ to 2π gives the Chern numbers of three bands, which is consistent with the $2\mathbb{Z}$ Chern number. This also provides a different way to understand the $2\mathbb{Z}$ quantization. In Fig. 1(d), we observe that the Berry phase for each band has a π period, which is proved in Appendix B. Due to the quantization of Berry phase at $\phi_L = 0$ and π, the accumulation of Berry phases must also be quantized in $[0,\pi)$ and this is further doubled in the parameter space $[0,2\pi)$, leading to a $2\mathbb{Z}$ classification.

Finally, we remark that the summation of the normalized Berry phase always vanishes (for both odd and even q), which suggests that the global Berry phase used in studying similar 1D non-Hermitian systems [47,61] does not apply here. The topological invariant (Chern number and the following $\mathbb{Z}_2$ invariant) always sums to zero as the non-Hermiticity here does not affect the additivity in *sum rule* [62]. This is a well-defined 2D non-Hermitian topological insulator characterized by a $2\mathbb{Z}$ Chern number and could be realized in a 1D lattice with only non-Hermitian modulations.

C. $\mathbb{Z}_2$ topological semimetal

We now consider $\alpha = \frac{1}{4}$ and the corresponding 2D band structure in momentum-parameter space is shown in Fig. 2(a). The spectrum obeys the symmetry $\omega(k) = \omega^*(-k)$ and is

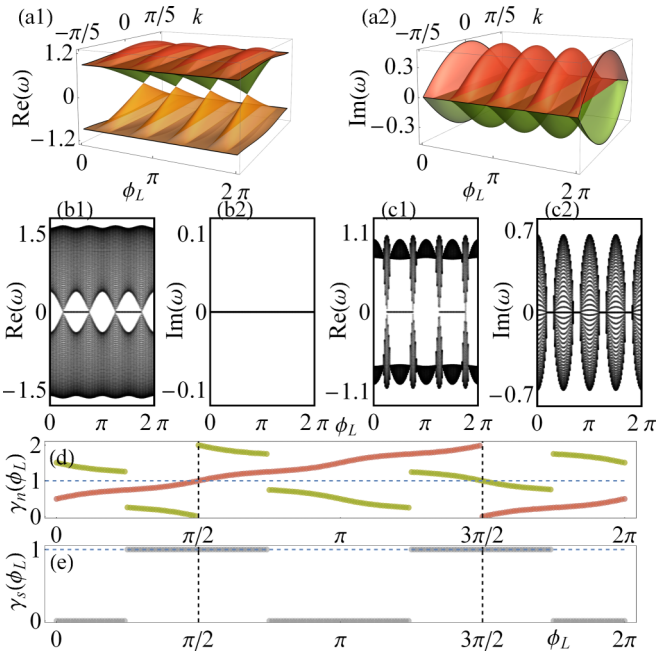

FIG. 2. $\mathbb{Z}_2$ topological semimetal phase when $\alpha = \frac{1}{4}$. (a) 2D band structure in momentum-parameter space when $\lambda = 1.1$. Open-boundary spectrum with respect to ϕ_L for (b) weak $\lambda = 0.8$ and (c) strong $\lambda = 1.2$ non-Hermitian modulations. We set $N_L = 120$ in the spatial direction. (d) Normalized Berry phase $\gamma_n(\phi_L)$ for bulk bands in (b). (e) The $\mathbb{Z}_2$ invariant computed from (d). The dashed vertical lines indicate inversion-symmetric points.

symmetric about $\omega = 0$. The latter results from an additional sublattice symmetry $\mathcal{C} = I_{q/2}\otimes\sigma_z$ with $\mathcal{C}^{-1}H(k,\phi_L)\mathcal{C} = -H(k,\phi_L)$ when q is even. Such a symmetry allows a finite band gap at zero energy and is well known for supporting zero-energy modes in 1D Hermitian systems (also known as chiral symmetry in Hermitian system). The spectrum is gapped everywhere in the momentum-parameter space except at a few high-symmetry points, where Dirac fermions emerge. This naturally makes the system a semimetal. These complex Dirac points are nontrivial and can be characterized by the normalized Berry phase $\frac{1}{\pi}\oint_L dk\,d\phi_L\mathcal{A}_{k,\phi_L}^n = 1$, where L is a loop encircling the complex Dirac point.

The open-boundary energy levels with respect to ϕ_L are given in Figs. 2(b) and 2(c). The spectrum is real for a weak modulation strength λ and the twofold-degenerate edge modes have exact zero and purely real energy despite the underlying non-Hermiticity of the system. The gap-closing points at certain inversion-symmetric points of ϕ_L and $k = 0$ are the complex Dirac point in Fig. 2(a) and represent topological phase transition in the 1D picture.

The topological invariant associated with these zero modes comes from the normalized Berry phases $\gamma_n(\phi_L)$ that are computed numerically in Fig. 2(d). Only the quantization of Berry phase at inversion-symmetric points survives because it does not require a gapped bulk (see Appendix B for details). The two bands $\mathrm{Re}(\omega) > 0$ (the particle branch) have the same Berry phases as the two with $\mathrm{Re}(\omega) < 0$ (the hole branch). We define the $\mathbb{Z}_2$ invariant $\gamma_s(\phi_L) = \sum_j \gamma_{n,j}(\phi_L)$ mod 2, where the summation runs over the hole branch and

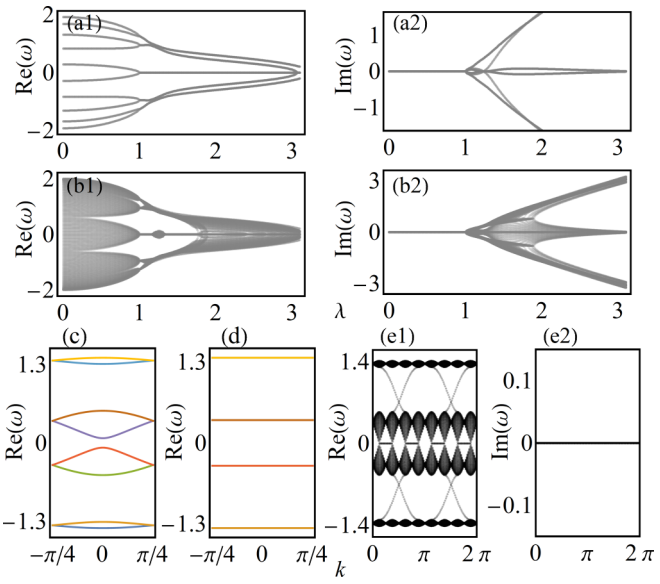

FIG. 3. (a) Open-boundary spectrum with respect to λ for $\alpha = \frac{1}{5}$, $\phi_L = 0$, and $N_L = 10$. (b) Similar to (a) except $N_L = 120$. (c) Bulk bands when $\alpha = \frac{1}{8}$, $\lambda = 1$, and $\phi_L = 0.1\pi$. (d) Flat bands at high-symmetry points $\phi_L = \pi/4$. Other parameters are the same as (c). (e) Coexistence of chiral surface wave and zero modes at $\alpha = \frac{1}{8}$ and $\lambda = 1$.

$\gamma_s(\phi_L) = 1/0$ corresponds to the topological or trivial phase. We find $\gamma_s(\phi_L) = 1$ in the region $\frac{1}{4}\pi < \phi_L < \frac{3}{4}\pi$ and $\frac{5}{4}\pi < \phi_L < \frac{7}{4}\pi$, and 0 otherwise [see Fig. 2(e)], which agree with the edge states and gap closing in Figs. 2(a)–2(c). Since the bulk bands could be degenerate at high-symmetric points, we apply an infinitesimal $\delta\phi_L$ in the hopping term $t_{i+1,i}$ to break the degeneracy so that both the Berry phases and $\mathbb{Z}_2$ invariant can be well defined (see Appendix C). Such a small perturbation does not break the sublattice symmetry, therefore, it does not affect the topological properties discussed in this section.

Finally, we remark that an alternative definition of the $\mathbb{Z}_2$ invariant is to use the normalized non-Abelian Berry phase and take partial trace over the hole branch. This does not require the gap-lifting term but leads to the same result as that in Fig. 2(e).

D. Robust $\mathcal{PT}$-symmetric-like and mixing phases

The open-boundary spectrum is surprisingly real when the Bloch bands in the Brillouin zone are imaginary, which is very different from most non-Hermitian systems and is a result of the robust $\mathcal{PT}$-symmetric-like phase. The $\mathcal{PT}$ symmetry is generally fragile in the sense that the critical value of driving term becomes very small when the system size is very large [63] (see also Appendix D). In contrast, the $\mathcal{PT}$-symmetric-like phase here is robust and cannot be spontaneously broken when $\lambda < 1$ regardless of the chain length N_L. As an example, we show the spectrum of an open chain with different length N_L in Figs. 3(a) and 3(b). The spectrum becomes complex at a fixed modulation strength $\lambda = 1$ for both $N_L = 10$ and 120. This notable feature of robust $\mathcal{PT}$-symmetric-like phases ensures the reality of both bulk spectrum and edge modes in an extended parameter space.

To get insights of the $\mathcal{PT}$-symmetric-like phase, we consider two-level systems with the following two non-Hermitian Hamiltonians $H_{\rm gl} = \sigma_y + i\lambda_\gamma\sigma_z, \lambda_\gamma \in \mathbb{R}$ and $H_{\rm ah} = \sigma_x + i\lambda_\mu\sigma_y, \lambda_\mu \in \mathbb{R}$. The former one defines the simplest $\mathcal{PT}$-symmetric model with balanced gain and loss while the latter one corresponds to the asymmetric hopping discussed in this work. It is obvious that $H_{\rm ah}$ is equivalent to $H_{\rm gl}$ through basis rotation $\sigma_x \to \sigma_z$, $\sigma_y \to \sigma_x$, and $\sigma_z \to \sigma_y$, which explains the $\mathcal{PT}$-symmetric-like phase in our system. The robustness, namely, the site-independent critical gain and loss rate, is discussed in Appendix D.

The $2\mathbb{Z}$ Chern insulator exists for any $q > 2$, while the topological semimetal requires sublattice symmetry and even q, which suggest that these two distinct phases can mix for a large even q. We consider $\alpha = \frac{1}{8}$ and the Bloch band is plotted in Fig. 3(c), which also exhibits flat band at high-symmetry points in the parameter space as shown in Fig. 3(d). The real open-boundary spectrum for the mixed phase is shown in Fig. 3(e). The topological properties can be similarly characterized by taking into account of band degeneracy (see Appendix E for details).

III. DISCUSSION AND CONCLUSION

Our model uses non-Hermitian nearest-neighbor hoppings on a lattice structure with uniform onsite potential. This could be realized in platforms like cold atoms in optical lattice or array of coupled waveguides. Many schemes have been proposed to realize asymmetric hoppings in both platforms [53,64]. Here, we briefly illustrate the experimental considerations with photonic crystals.

When the non-Hermitian (or asymmetric) hopping is turned off, the model can be realized by a 1D array of optical microring cavities with equal spacing. To induce the non-Hermitian effects, we first evanescently couple the ring cavities to their nearest neighbors through a set of auxiliary rings, and then add gain and loss to each side of the auxiliary rings, which can be realized through coating or doping [64–66]. Because the auxiliary rings can be controlled individually, both the non-Hermitian Chern insulator and the topological semimetal phases are accessible. In this sense, we are dealing with bosonic systems and the topological modes are robust to fabrication imperfections. To observe the topological modes, we excite the edge modes by controlled laser source, or we can prompt the topological modes to lasing modes [45].

A few sites with small period $q = 2$ or 4 are sufficient for versatile topological phases (see Appendix C) and it is readily accessible in current experiments. The chiral edge waves and zero-energy modes have real energies in broad parameter spaces, therefore, they are free of dissipations and amplifications over time and are easier to observe in experiments comparing to imaginary edge modes in many other models [47,63].

There are many other non-Hermitian topological phases that could be explored in this system by considering, for instance, other types of non-Hermitian hoppings, staggered V_i, tilted lattice, and long-range hopping. These ingredients could bring richer physics as demonstrated already in certain bipartite superlattice [34,37,38].

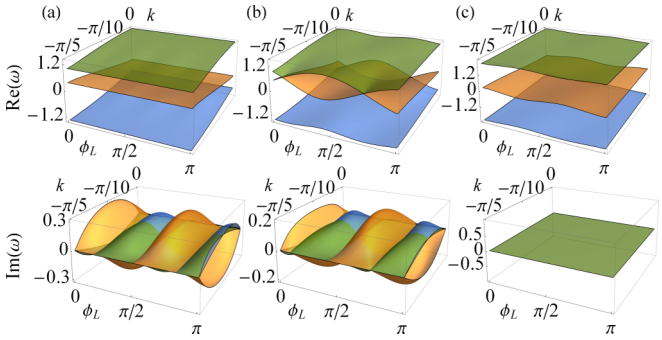

FIG. 4. (a) Band structure for $2\mathbb{Z}$ Chern insulator phase shown in Fig. 1(b). The band Chern numbers are -2, 4, and -2 from bottom to top. (b) Real gap closing at $\delta\phi_L = 0.16\pi$. (c) Band structure for $\mathbb{Z}$ Chern insulator phase shown in Fig. 1(c). The band Chern numbers are -1, 2, and -1 from bottom to top.

In conclusion, we show that two unique non-Hermitian 2D topological phases, a $2\mathbb{Z}$ Chern insulator and a $\mathbb{Z}_2$ topological semimetal, can be realized in a 1D lattice with staggered non-Hermitian hoppings. These phases can be experimentally realized in photonic or atomic systems and may open an avenue for exploring unique classes of non-Hermitian topological phases with 1D superlattices.

ACKNOWLEDGMENTS

J.H. and C.Z. are supported by Air Force Office of Scientific Research (Grants No. FA9550-16-1-038 and No. FA9550-20-1-0220), National Science Foundation (Grant No. PHY-1806227), and Army Research Office (Grant No. W911NF-17-1-0128). Y.-J.W. is supported in part by NSFC under the Grant No. 11504285 and the Scientific Research Program Funded by Natural Science Basic Research Plan in Shaanxi Province of China (Program No. 2018JQ1058).

APPENDIX A: TOPOLOGICAL PHASE TRANSITION FROM $2\mathbb{Z}$ TO $\mathbb{Z}$ CHERN INSULATOR

As we discussed in the main text, the $\delta\phi_L$ term breaks relevant symmetries protecting the non-Hermitian $2\mathbb{Z}$ Chern insulator phase, rendering a $\mathbb{Z}$ classification. The corresponding topological phase transition is demonstrated in Fig. 4.

Figures 4(a) and 4(c) show, respectively, the real and imaginary band structures in momentum-parameter space for Figs. 1(b) and 1(c). While these two phases cannot be continuously deformed from one to the other, a real gap closing is observed in Fig. 4(b) near $\delta\phi_L = 0.16\pi$. This further justifies that the $2\mathbb{Z}$ Chern insulator phase is topologically distinct from the $\mathbb{Z}$ Chern insulator phase.

APPENDIX B: PROOF OF BERRY PHASE PERIODICITY AND QUANTIZATION AND THE $2\mathbb{Z}$ CHERN NUMBER

In the main text, a few statements are made based upon physical considerations and are supported with numerics. Here, more rigorous proofs are provided for some important statements. In this section, we denote $k_y \equiv \phi_L$ to write the momentum-parameter space (k, ϕ_L) as $\mathbf{k} = (k_x, k_y)$ for easy notation.

The right and left eigenvectors are defined as

$$H(\mathbf{k})|\psi(\mathbf{k})\rangle_R = \omega(\mathbf{k})|\psi(\mathbf{k})\rangle_R,$$
$$H(\mathbf{k})^\dagger|\psi(\mathbf{k})\rangle_L = \omega^*(\mathbf{k})|\psi(\mathbf{k})\rangle_L, \tag{B1}$$

with the normalization condition ${}_L\langle\psi(\mathbf{k})|\psi(\mathbf{k})\rangle_R = 1$. There are four different definitions of Berry connection $\mathcal{A}^{ab}_{\mathbf{k}} = -i_a\langle\psi|\partial_{\mathbf{k}}\psi\rangle_b$, where $a, b = L, R$. A natural generalization from Hermitian systems would be $\mathcal{A}^{LR}_{\mathbf{k}}$, which is not generally correct. While $\mathcal{A}^{aa}_{\mathbf{k}}$ is always real because ${}_a\langle\psi|\partial_{\mathbf{k}}\psi\rangle_a$ is purely imaginary due to the normalization condition, $\mathcal{A}^{ab}_{\mathbf{k}}, a \neq b$ could be any complex number since the normalization condition only restricts ${}_a\langle\psi|\partial_{\mathbf{k}}\psi\rangle_b + {}_a\langle\partial_{\mathbf{k}}\psi|\psi\rangle_b = 0$. To resolve this, we consider a normalized Berry connection

$$\mathcal{A}^n_{\mathbf{k}} = \tfrac{1}{2}\left(\mathcal{A}^{RL}_{\mathbf{k}} + \mathcal{A}^{LR}_{\mathbf{k}}\right), \tag{B2}$$

which is purely real because $\mathcal{A}^n_{\mathbf{k}} - \mathcal{A}^{n*}_{\mathbf{k}} = -\frac{i}{2}({}_R\langle\psi|\partial_{\mathbf{k}}\psi\rangle_L + {}_L\langle\psi|\partial_{\mathbf{k}}\psi\rangle_R + {}_R\langle\partial_{\mathbf{k}}\psi|\psi\rangle_L) = -\frac{i}{2}\partial_{\mathbf{k}}({}_R\langle\psi|\psi\rangle_L + {}_L\langle\psi|\psi\rangle_R) = 0$ or simply $\mathcal{A}^{LR}_{\mathbf{k}} = (\mathcal{A}^{RL}_{\mathbf{k}})^*$. Such a well-defined Berry connection yields a (normalized) Berry phase $\gamma_n = \frac{1}{\pi}\oint d\mathbf{k}\cdot\mathcal{A}^n_{\mathbf{k}}$, which is real and quantized along a closed loop for any gapped non-Hermitian systems.

We now show that such a Berry phase $\gamma_n(k_y) = \frac{1}{\pi}\oint dk_x\mathcal{A}^n_{k_x}(k_y)$ would have a period T if $H(k_x, k_y) = H^\dagger(k_x, k_y + T)$ and the bands are real and gapped (a weaker condition is that the bands are separable by their real parts). Starting with the definition of left eigenvector in Eq. (B1) and applying the aforementioned conditions, we have $H(k_x, k_y)|\psi(k_x, k_y + T)\rangle_L = \omega^*(k_x, k_y + T)|\psi(k_x, k_y + T)\rangle_L$ so that $\mathcal{A}^{RL}_{k_x}(k_y) = \mathcal{A}^{LR}_{k_x}(k_y + T)$ and vice versa. Now, we realize that $\mathcal{A}^n_{k_x}(k_y) = \frac{1}{2}[\mathcal{A}^{RL}_{k_x}(k_y) + \mathcal{A}^{LR}_{k_x}(k_y)] = \frac{1}{2}[\mathcal{A}^{LR}_{k_x}(k_y + T) + \mathcal{A}^{RL}_{k_x}(k_y + T)] = \mathcal{A}^n_{k_x}(k_y + T)$. Integrating along k_x, we find the Berry phase has a similar periodicity $\gamma_n(k_y) = \gamma_n(k_y + T)$. Another consequence here is that the Chern number will be the multiple of some integers due to the periodicity of Berry connection. We could also define a normalized Chern number C^n based on the normalized Berry connection so that

$$\begin{aligned} C^n &= \frac{1}{2\pi}\oint dk_x dk_y\left(\partial_{k_x}\mathcal{A}^n_{k_y} - \partial_{k_y}\mathcal{A}^n_{k_x}\right) \\ &= \frac{1}{2}\left(\frac{1}{2\pi}\oint dk_x dk_y\left(\partial_{k_x}\mathcal{A}^{RL}_{k_y} - \partial_{k_y}\mathcal{A}^{RL}_{k_x}\right)\right. \\ &\quad \left. + \frac{1}{2\pi}\oint dk_x dk_y\left(\partial_{k_x}\mathcal{A}^{LR}_{k_y} - \partial_{k_y}\mathcal{A}^{LR}_{k_x}\right)\right) \\ &= \frac{1}{2}(C^{RL} + C^{LR}) \\ &= C^{ab}. \end{aligned} \tag{B3}$$

As $C^n_T = \frac{1}{2\pi}\oint dk_x\int_{k_y}^{k_y+T} dk_y(\partial_{k_x}\mathcal{A}^n_{k_y} - \partial_{k_y}\mathcal{A}^n_{k_x})$ must be quantized due to the quantized charge pumping along k_y demanded by the periodicity of the Berry phase, it is easy to see $C^n = N_y C^n_T$ belongs to a $N_y\mathbb{Z}$ class if k_y has the period $k_y = k_y + N_y T$.

We also claim that the Berry phase is quantized at inversion-symmetric points. To show this, we consider the symmetry $\mathcal{I}_k H(k_x, k_y)\mathcal{I}_k^{-1} = H(-k_x, -k_y + T)$. Such a symmetry dictates $H(k_x, k_y)|\mathcal{I}_k\psi(-k_x, -k_y + T)\rangle_R = \omega(-k_x, -k_y + T)|\mathcal{I}_k\psi(-k_x, -k_y + T)\rangle_R$. When the system is gapped, we have $\mathcal{A}^n_{k_x}(k_y) = \mathcal{A}^n_{-k_x}(-k_y + T)$, where the condition $\mathcal{I}_k^2 = I$ is used. Then, the Berry phase reads as $\gamma_n(k_y) = \frac{1}{\pi}\oint dk_x \mathcal{A}^n_{k_x}(k_y) = \frac{1}{\pi}\oint dk_x \mathcal{A}^n_{-k_x}(-k_y + T) = -\frac{1}{\pi}\oint dk_x \mathcal{A}^n_{k_x}(-k_y + T) = -\gamma_n(-k_y + T)$. This implies that $\gamma_n(k'_y) = -\gamma_n(k'_y)$ if $k'_y = k'_y - T$ (i.e., the high-symmetry point), which means it can only take the quantized value 0 or 1.

We now go back to the specific model we discussed in the main text, where $T = \pi$ and $k_y = \phi_L$ has a period 2π ($N_y = 2$). This means that the Berry phase satisfies $\gamma_n(\phi_L) = \gamma_n(\phi_L \pm \pi)$ and the Chern insulator has a Chern number $2\mathbb{Z}$ which is determined by the symmetry $H(k, \phi_L) = H^\dagger(k, \phi_L + \pi)$. Another constraint on Berry phase is $\gamma_n(\phi_L) = -\gamma_n(-\phi_L \pm \pi)$ so that it is quantized at inversion-symmetric point $\phi_L = \pm\frac{\pi}{2}$. Combining the two conditions together, we find further $\gamma_n(\phi_L) = \gamma_n(\phi_L + \pi) = -\gamma_n(-\phi_L)$ and, thus, the Berry phase is also quantized at $\phi_L = 0$ and π. Note that the last relation is imposed by the $\mathcal{Q}$ symmetry, which can be similarly proved if the bulk band is gapped in the real part.

APPENDIX C: LIFTING BAND DEGENERACIES IN TOPOLOGICAL SEMIMETAL

In the topological semimetal phase, there could be band degeneracy in momentum space, which hinders the computation of Berry phase or $\mathbb{Z}_2$ invariant. In the following, we take the example $\alpha = \frac{1}{4}$ for illustration purpose. The Bloch Hamiltonian reads as

$$\begin{aligned} H = &\frac{1 + \cos(4k) + i\lambda\ \sin(4k)\cos(\phi_L)}{2}\sigma_x \otimes \sigma_x \\ &+ \frac{1 - \cos(4k) - i\lambda\ \sin(4k)\cos(\phi_L)}{2}\sigma_y \otimes \sigma_y \\ &+ \frac{\sin(4k) + i\lambda\ \cos(\phi_L)(1 - \cos(4k))}{2}\sigma_x \otimes \sigma_y \\ &+ \frac{\sin(4k) - i\lambda\ \cos(\phi_L)(1 + \cos(4k))}{2}\sigma_y \otimes \sigma_x. \end{aligned} \tag{C1}$$

The bulk bands are

$$E_{\pm,\pm} = \pm\sqrt{2 - \lambda^2 \pm \sqrt{\tfrac{1}{2}\{8 - 8\lambda^2 + \lambda^4[1 - \cos(4\phi_L)]\}}} \tag{C2}$$

at the high-symmetry point $k = 0$. We notice that when $\cos(4\phi_L) = -1$, i.e., $\phi_L = \frac{1}{4}\pi, \frac{3}{4}\pi, \frac{5}{4}\pi, \frac{7}{4}\pi$, the band gap closes in momentum space with $E_{+,-} = E_{-,+} = 0$ and $E_{+,+} = -E_{-,-} = \sqrt{2(2 - \lambda^2)}$ when $\lambda < \sqrt{2}$, manifesting the topological phase transition that was discussed in the main text. There is always a degenerate point in the top $E_{+,\pm} = +\sqrt{2 - \lambda^2}$ and bottom $E_{-,\pm} = -\sqrt{2 - \lambda^2}$ two bands at $k = \frac{\pi}{4}$. Such a degeneracy prevents us from computing the topological invariant in momentum space, while it is irrelevant to the topological properties since it does not depend on ϕ_L. To resolve this, we apply a perturbation term on the asymmetric hopping

$$t_{i+1,i} = 1 - \lambda\ \cos(2\pi\alpha i + \phi_L + \delta\phi_L), \quad \delta\phi_L \in \mathbb{R} \tag{C3}$$

which perseveres the sublattice symmetry so that it would not change the associated topological invariant. It breaks the degeneracy at $k = \pi/4$ but preserves the gap closings at topological phase transition points.

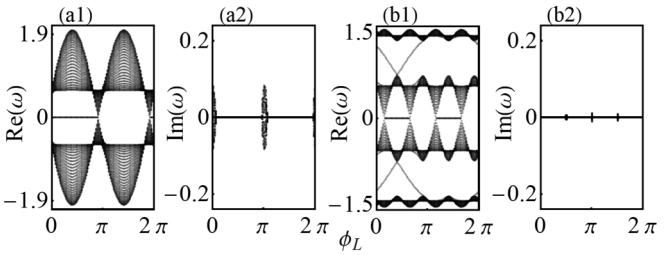

FIG. 5. (a) Open-boundary spectrum for varying ϕ_L with $\alpha = \frac{1}{2}$, $\lambda = 1$, and $\delta\phi_L = 0.2\pi$. (b) Similar as (a) but plotted with $\alpha = \frac{1}{4}$.

When a finite $\delta\phi$ is considered, a few interesting points arise. First, the topological semimetal phase can be realized in a two-level system, i.e., $\alpha = \frac{1}{2}$ [see Fig. 5(a)], which represents some non-Hermitian SSH models that have been discussed in previous literatures [37,38]. The $\mathbb{Z}_2$ index reduces to the 1D Zak phase of the ground state, which can correctly characterize the non-Hermitian SSH model with Hermitian chiral symmetry.

A finite $\delta\phi$ would spoil the $2\mathbb{Z}$ Chern number and, thus, renders a $\mathbb{Z}$-type Chern insulator. Moreover, since it breaks the degeneracy within the bottom and top two bands at $\alpha = \frac{1}{4}$, respectively, there would be a gap opening, providing the possibility of supporting a nontrivial Chern insulator phase. We demonstrate these two points in Fig. 5(b), where we do observe one chiral surface wave (for a given propagating direction) residing within each gap. The zero modes naturally persist but are shifted with the topological phase transition points. The characterization of the topological properties are similar and a case study of a mix phase is presented in Appendix E.

APPENDIX D: $\mathcal{PT}$-SYMMETRIC PHASE BY GAIN AND LOSS IS FRAGILE

In main text, we state that the usual $\mathcal{PT}$-symmetric phase by gain and loss is fragile, therefore, the spectrum cannot be purely real in the separable regime [63]. To illustrate the fragile $\mathcal{PT}$-symmetric phase, we consider a simple model described by the following tight-binding Hamiltonian:

$$H_{\mathcal{PT}} = t\sum_i(\hat{c}_i^\dagger\hat{c}_{i+1} + \text{H.c.}) + (-1)^i\gamma\hat{c}_i^\dagger\hat{c}_i, \tag{D1}$$

where $\gamma > 0$ is onsite gain and loss rate. The Hamiltonian is defective at the exceptional point and the system enters the partially broken regime (part of the spectrum becomes complex) at the smallest γ_c satisfying $\text{Det}(H_{\mathcal{PT}}(\gamma_c)) = 0$. The determinant can be solved through the recursive equation $D_n = (-1)^n\gamma D_{n-1} - t^2 D_{n-2}$ with boundary conditions $D_1 = -i\gamma$ and $D_2 = \gamma^2 - t^2$. The critical values γ_c for different chain lengths are shown in Fig. 6, where we see a fast drop

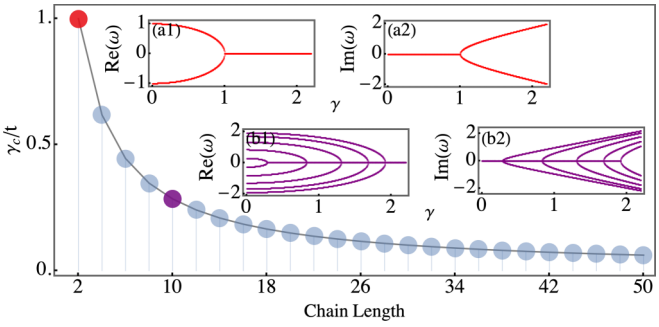

FIG. 6. Critical gain and loss rate for $\mathcal{PT}$ breaking versus the length of the total chain in real space. The insets show how the spectrum changes for varying γ at given chain length 2 or 10.

of γ_c when the chain length starts to increase and ultimately approaches zero. In the insets (a) and (b), we show the spectrum for varying γ at different chain lengths 2 and 10. This argument also applies to more general cases such as larger unit cell, quasiperiodic potential, or higher dimensions. This explains the complex edge states observed in many models with onsite gain and loss [47,63].

Such a fragility does not happen when the non-Hermiticity is introduced by asymmetric hopping as illustrated in Figs. 3(a) and 3(b), thus, our model enjoys real edge modes and is more accessible to experimental observation. To get more insights into the robustness, we simplify our model by assuming an equal-spacing lattice with non-Hermitian nearest-neighbor hopping $t \pm \lambda$, where $t, \lambda \in \mathbb{R}$. Similar to the above analyses, we solve the determinant of the system, which turns out to be $D_n = 0$ and $D_n = (\gamma^2 - t^2)^{(n/2)}$ for odd and even n, respectively. The cases with odd n always have vanishing determinant. We also notice that all the "exceptional points" collapse to one pair $\gamma_c = \pm t$, which is independent of n when n is even. Such independence is ascribed to the robustness of this $\mathcal{PT}$-symmetric-like phase. We also remark that a system with odd sites must also have the same critical points because γ_c is continuous in the thermodynamic limits.

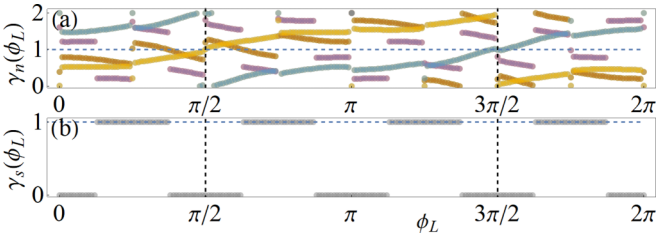

FIG. 7. (a) Berry phase $\gamma_n(\phi_L)$ for the coexisting phase shown in Fig. 3(e). The dashed vertical lines indicate inversion-symmetric points and the numeric errors are more significant near gap-closing points. (b) The $\mathbb{Z}_2$ invariant computed from (a).

APPENDIX E: TOPOLOGICAL CHARACTERIZATION OF THE COEXISTING PHASE

Although we have studied two topological phases individually, the coexisting phase can be characterized in a similar way if the band degeneracy is treated carefully. We still consider a small perturbation $\delta\phi_L$ when we compute the Berry phase and the results are shown in Fig. 7(a). Due to the gapless phase, the Berry phase does not have the periodicity any more. However, it is still quantized at inversion-symmetric point because a small $\delta\phi_L$ only perturbs the system slightly. In Fig. 3(e), the chiral surface wave still crosses at the high-symmetry points, at which the Berry phases are quantized to nontrivial values [Fig. 7(a)].

We notice that the Chern number is not well defined due to the topological phase transition point and degeneracies between top and bottom four bands. While $\delta\phi_L$ term allows computing the Chern number, it breaks the $2\mathbb{Z}$ constraint, and the Chern numbers are odd for the top and bottom two bands [see also the charge pumping in Fig. 7(a)]. When $\delta\phi_L$ is gradually tuned to 0, the band Chern number should not change because there is no topological phase transition. When $\delta\phi_L = 0$, two bands become degenerate. If we take both bands as a single band, the Chern number is even and the chiral surface wave appears in pair in each gap.

In comparison, the zero modes can be directly characterized by the $\mathbb{Z}_2$ invariant, which is shown in Fig. 7(b), and it is consistent with the zero modes observed in Fig. 3(e).

[1] D. Xiao, M.-C. Chang, and Q. Niu, Berry phase effects on electronic properties, Rev. Mod. Phys. **82**, 1959 (2010).

[2] C.-K. Chiu, J. C. Y. Teo, A. P. Schnyder, and S. Ryu, Classification of topological quantum matter with symmetries, Rev. Mod. Phys. **88**, 035005 (2016).

[3] J. Wang and S.-C. Zhang, Topological states of condensed matter, Nat. Mater. **16**, 1062 (2017).

[4] M. Aidelsburger, M. Atala, M. Lohse, J. T. Barreiro, B. Paredes, and I. Bloch, Realization of the Hofstadter Hamiltonian with Ultracold Atoms in Optical Lattices, Phys. Rev. Lett. **111**, 185301 (2013).

[5] M. Atala, M. Aidelsburger, J. T. Barreiro, D. Abanin, T. Kitagawa, E. Demler, and I. Bloch, Direct measurement of the Zak phase in topological Bloch bands, Nat. Phys. **9**, 795 (2013).

[6] M. Aidelsburger, M. Lohse, C. Schweizer, M. Atala, J. T. Barreiro, S. Nascimbène, N. R. Cooper, I. Bloch, and N. Goldman, Measuring the Chern number of Hofstadter bands with ultracold bosonic atoms, Nat. Phys. **11**, 162 (2014).

[7] G. Jotzu, M. Messer, R. Desbuquois, M. Lebrat, T. Uehlinger, D. Greif, and T. Esslinger, Experimental realization of the topological Haldane model with ultracold fermions, Nature (London) **515**, 237 (2014).

[8] M. Lohse, C. Schweizer, O. Zilberberg, M. Aidelsburger, and I. Bloch, A Thouless quantum pump with ultracold bosonic atoms in an optical superlattice, Nat. Phys. **12**, 350 (2015).

[9] S. Nakajima, T. Tomita, S. Taie, T. Ichinose, H. Ozawa, L. Wang, M. Troyer, and Y. Takahashi, Topological Thouless pumping of ultracold fermions, Nat. Phys. **12**, 296 (2016).

[10] N. Goldman, J. C. Budich, and P. Zoller, Topological quantum matter with ultracold gases in optical lattices, Nat. Phys. **12**, 639 (2016).

[11] N. R. Cooper, J. Dalibard, and I. B. Spielman, Topological Bands for Ultracold Atoms, Rev. Mod. Phys. **91**, 015005 (2019).

[12] F. D. M. Haldane and S. Raghu, Possible Realization of Directional Optical Waveguides in Photonic Crystals with Broken Time-Reversal Symmetry, Phys. Rev. Lett. **100**, 013904 (2008).

[13] Z. Wang, Y. Chong, J. D. Joannopoulos, and M. Soljacic, Observation of unidirectional backscattering-immune topological electromagnetic states, Nature (London) **461**, 772 (2009).

[14] L. Lu, C. Fang, L. Fu, S. G. Johnson, J. D. Joannopoulos, and M. Soljačić, Symmetryed topological photonic crystal in three dimensions, Nat. Phys. **12**, 337 (2010).

[15] L. Lu, J. D. Joannopoulos, and M. Soljacic, Topological photonics, Nat. Photonics **8**, 821 (2014).

[16] A. B. Khanikaev and G. Shvets, Two-dimensional topological photonics, Nat. Photonics **11**, 763 (2014).

[17] G. Siroki, P. A. Huidobro, and V. Giannini, Topological photonics: From crystals to particles, Phys. Rev. B **96**, 041408(R) (2017).

[18] B. Bahari, A. Ndao, F. Vallini, A. E. Amili, Y. Fainman, and B. Kanté, Nonreciprocal lasing in topological cavities of arbitrary geometries, Science **358**, 636 (2017).

[19] C. He, X. Ni, H. Ge, X.-C. Sun, Y.-B. Chen, M.-H. Lu, X.-P. Liu, and Y.-F. Chen, Acoustic topological insulator and robust one-way sound transport, Nat. Phys. **12**, 1124 (2016).

[20] H. He, C. Qiu, L. Ye, X. Cai, X. Fan, M. Ke, F. Zhang, and Z. Liu, Topological negative refraction of surface acoustic waves in a Weyl phononic crystal, Nature (London) **560**, 61 (2018).

[21] S. Imhof, C. Berger, F. Bayer, J. Brehm, L. W. Molenkamp, T. Kiessling, F. Schindler, C. H. Lee, M. Greiter, T. Neupert, and R. Thomale, Topolectrical-circuit realization of topological corner modes, Nat. Phys. **14**, 925 (2018).

[22] J.-H. Wu, M. Artoni, and G. C. La Rocca, Non-Hermitian Degeneracies and Unidirectional Reflectionless Atomic Lattices, Phys. Rev. Lett. **113**, 123004 (2014).

[23] M. Kreibich, J. Main, H. Cartarius, and G. Wunner, Realizing PT-symmetric non-Hermiticity with ultracold atoms and Hermitian multiwell potentials, Phys. Rev. A **90**, 033630 (2014).

[24] J. Li, A. K. Harter, J. Liu, L. de Melo, Y. N. Joglekar, and L. Luo, Observation of parity-time symmetry breaking transitions in a dissipative Floquet system of ultracold atoms, Nat. Commun. **10**, 855 (2019).

[25] F. Mostafavi, L. Yuan, and H. Ramezani, Eigenstates Transition without Undergoing an Adiabatic Process, Phys. Rev. Lett. **122**, 050404 (2019).

[26] L. Pan, S. Chen, and X. Cui, Interacting non-Hermitian ultracold bosonic systems in three-dimensional harmonic trap: Two-body exact solutions and high-order exceptional points, Phys. Rev. A **99**, 063616 (2019).

[27] K. Yamamoto, M. Nakagawa, K. Adachi, K. Takasan, M. Ueda, and N. Kawakami, Theory of Non-Hermitian Fermionic Superfluidity with a Complex-Valued Interaction, Phys. Rev. Lett. **123**, 123601 (2019).

[28] K. G. Makris, R. El-Ganainy, D. N. Christodoulides, and Z. H. Musslimani, Beam Dynamics in PT Symmetric Optical Lattices, Phys. Rev. Lett. **100**, 103904 (2008).

[29] A. Regensburger, C. Bersch, M.-A. Miri, G. Onishchukov, D. N. Christodoulides, and U. Peschel, Parity–time synthetic photonic lattices, Nature (London) **488**, 167 (2012).

[30] B. Peng, S. K. Özdemir, S. Rotter, H. Yilmaz, M. Liertzer, F. Monifi, C. M. Bender, F. Nori, and L. Yang, Loss-induced suppression and revival of lasing, Science **346**, 328 (2012).

[31] J. M. Zeuner, M. C. Rechtsman, Y. Plotnik, Y. Lumer, S. Nolte, M. S. Rudner, M. Segev, and A. Szameit, Observation of a Topological Transition in the Bulk of a Non-Hermitian System, Phys. Rev. Lett. **115**, 040402 (2015).

[32] L. Feng, R. El-Ganainy, and L. Ge, Non-Hermitian photonics based on parity–time symmetry, Nat. Photonics **11**, 752 (2017).

[33] J. Hou, Z. Li, Q. Gu, and C. Zhang, Non-Hermitian photonics based on charge-parity symmetry, arXiv:1904.05260.

[34] T. E. Lee, Anomalous Edge State in a Non-Hermitian Lattice, Phys. Rev. Lett. **116**, 133903 (2016).

[35] F. K. Kunst, E. Edvardsson, J. C. Budich, and E. J. Bergholtz, Biorthogonal Bulk-Boundary Correspondence in Non-Hermitian Systems, Phys. Rev. Lett. **121**, 026808 (2018).

[36] S. Yao, F. Song, and Z. Wang, Non-Hermitian Chern Bands, Phys. Rev. Lett. **121**, 136802 (2018).

[37] S. Yao and Z. Wang, Edge States and Topological Invariants of Non-Hermitian Systems, Phys. Rev. Lett. **121**, 086803 (2018).

[38] S. Lieu, Topological phases in the non-Hermitian Su-Schrieffer-Heeger model, Phys. Rev. B **97**, 045106 (2018).

[39] H. Shen, B. Zhen, and L. Fu, Topological Band Theory for Non-Hermitian Hamiltonians, Phys. Rev. Lett. **120**, 146402 (2018).

[40] L. Jin and Z. Song, Bulk-boundary correspondence in a non-Hermitian system in one dimension with chiral inversion symmetry, Phys. Rev. B **99**, 081103(R) (2019).

[41] K. Kawabata, S. Higashikawa, Z. Gong, Y. Ashida, and M. Ueda, Topological unification of time-reversal and particle-hole symmetries in non-Hermitian physics, Nat. Commun. **10**, 297 (2019).

[42] S. Lin, L. Jin, and Z. Song, Symmetryed topological phases characterized by isolated exceptional points, Phys. Rev. B **99**, 165148 (2019).

[43] S. Malzard, C. Poli, and H. Schomerus, Topologicallyed Defect States in Open Photonic Systems with Non-Hermitian Charge-Conjugation and Parity-Time Symmetry, Phys. Rev. Lett. **115**, 200402 (2015).

[44] P. St-Jean, V. Goblot, E. Galopin, A. Lemaître, T. Ozawa, L. Le Gratiet, I. Sagnes, J. Bloch, and A. Amo, Lasing in topological edge states of a one-dimensional lattice, Nat. Photonics **11**, 651 (2017).

[45] M. A. Bandres, S. Wittek, G. Harari, M. Parto, J. Ren, M. Segev, D. N. Christodoulides, and M. Khajavikhan, Topological insulator laser: Experiments, Science **359**, eaar4005 (2018).

[46] M. Parto, S. Wittek, H. Hodaei, G. Harari, M. A. Bandres, J. Ren, M. C. Rechtsman, M. Segev, D. N. Christodoulides, and M. Khajavikhan, Edge-Mode Lasing in 1D Topological Active Arrays, Phys. Rev. Lett. **120**, 113901 (2018).

[47] K. Takata and M. Notomi, Photonic Topological Insulating Phase Induced Solely by Gain and Loss, Phys. Rev. Lett. **121**, 213902 (2018).

[48] H. Zhou, C. Peng, Y. Yoon, C. W. Hsu, K. A. Nelson, L. Fu, J. D. Joannopoulos, M. Soljačić, and B. Zhen, Observation of bulk Fermi arc and polarization half charge from paired exceptional points, Science **359**, 1009 (2018).

[49] A. Cerjan, S. Huang, M. Wang, K. P. Chen, Y. Chong, and M. C. Rechtsman, Experimental realization of a Weyl exceptional ring, Nature Photon. **13**, 623 (2019).

[50] J. Hou, Z. Li, X.-W. Luo, Q. Gu, and C. Zhang, Topological Bands and Triply-Degenerate Points in Non-Hermitian Hyperbolic Metamaterials, Phys. Rev. Lett. **124**, 073603 (2020).

[51] X.-W. Luo and C. Zhang, Higher-Order Topological Corner States Induced by Gain and Loss, Phys. Rev. Lett. **123**, 073601 (2019).

[52] Y. Xu, S.-T. Wang, and L.-M. Duan, Weyl Exceptional Rings in a Three-Dimensional Dissipative Cold Atomic Gas, Phys. Rev. Lett. **118**, 045701 (2017).

[53] T. Liu, Y.-R. Zhang, Q. Ai, Z. Gong, K. Kawabata, M. Ueda, and F. Nori, Second-Order Topological Phases in Non-Hermitian Systems, Phys. Rev. Lett. **122**, 076801 (2019).

[54] Ch. H. Lee, L. Li, and J. Gong, Hybrid higher-order skin-topological modes in non-reciprocal systems, Phys. Rev. Lett. **123**, 016805 (2019).

[55] Z. Gong, Y. Ashida, K. Kawabata, K. Takasan, S. Higashikawa, and M. Ueda, Topological Phases of Non-Hermitian Systems, Phys. Rev. X **8**, 031079 (2018).

[56] D. Bernard and A. LeClair, A classification of non-hermitian random matrices, *Statistical Field Theories*, NATO Science Series (Series II: Mathematics, Physics and Chemistry, edited by A. Cappelli and G. Mussardo, Vol. 73 (Springer, Dordrecht, 2002), pp. 207–214.

[57] K. Kawabata, K. Shiozaki, M. Ueda, and M. Sato, Symmetry and Topology in Non-Hermitian Physics, Phys. Rev. X **9**, 041015 (2019).

[58] L.-J. Lang, X. Cai, and S. Chen, Edge States and Topological Phases in One-Dimensional Optical Superlattices, Phys. Rev. Lett. **108**, 220401 (2012).

[59] K. Shiozaki and M. Sato, Topology of crystalline insulators and superconductors, Phys. Rev. B **90**, 165114 (2014).

[60] Q.-B. Zeng, Y.-B. Yang, and Y. Xu, Topological phases in non-Hermitian Aubry-André-Harper models, Phys. Rev. B **101**, 020201(R) (2020).

[61] S.-D. Liang and G.-Y. Huang, Topological invariance and global Berry phase in non-Hermitian systems, Phys. Rev. A **87**, 012118 (2013).

[62] Y. Hatsugai, Explicit Gauge Fixing for Degenerate Multiplets: A Generic Setup for Topological Orders, J. Phys. Soc. Jpn. **73**, 2604 (2004).

[63] C. Yuce, $\mathcal{PT}$ symmetric Aubry-Andre model, Phys. Lett. A **378**, 2024 (2014).

[64] S. Longhi, D. Gatti, and G. Della Valle, Robust light transport in non-Hermitian photonic lattices, Sci. Rep. **5**, 13376 (2015).

[65] M. Hafezi, E. A. Demler, M. D. Lukin, and J. M. Taylor, Robust optical delay lines with topological protection, Nat. Phys. **7**, 907 (2011).

[66] H. Zhao, P. Miao, M. H. Teimourpour, S. Malzard, R. El-Ganainy, H. Schomerus, and L. Feng, Topological hybrid silicon microlasers, Nat. Commun. **9**, 981 (2018).